ORIGINAL ARTICLE

Numerical model of seepage flows by reformulating finite element method based on new spherical Hankel shape functions

Sajedeh Farmani[1] · Mahnaz Ghaeini-Hessaroeyeh[1] · Saleh Hamzehei-Javaran[1]

Abstract

The water penetration in soil is investigated numerically using the finite element method (FEM) in a novel way. In the suggested method, new spherical Hankel shape functions are used and the finite element method is reformulated based on them. These new functions are obtained from the first and second kind of Bessel functions. The properties of Hankel shape functions lead to having more accuracy and robustness for the proposed method with low number of elements. To validate the suggested approach, at first, a boundary value problem is solved and the results are compared with the available analytical solution. Then, in order to prove the efficiency and applicability of the present model in the seepage problems, five examples including saturated and unsaturated flow in porous media are studied and the hydraulic head is calculated. Afterward, the results obtained from the classical and new method are compared together. The comparisons indicate that the suggested method with the low number of elements is more precise than the classic FEM with the same mesh.

Keywords Finite element method · Spherical Hankel shape functions · Bessel function · Seepage problems · Hydraulic head

Introduction

The seepage phenomenon is an important issue in soil mechanics and water engineering and generally is defined as the slow moving of a fluid in a porous medium. This problem is related to various fields such as water seepage through body of a dam and its foundation and also groundwater flows. To study these problems, the governing equation of the boundary value problems should be solved. This equation is obtained by combining Darcy's and continuity laws. By solving the mentioned equation, the potential variable or hydraulic head is calculated.

The numerical study of the seepage problems has been considered by many researchers. The analytical methods are applied when one problem has simple geometry and boundary conditions. However, when the computational domain boundary conditions are complicated, the numerical methods are more efficient and usually have suitable

precision for the modeling. In the literature, several works have been done in the field of leakage flow problems by the numerical methods. Juanes (2005) presented a variational multiscale finite element method for multiphase flow in a porous media. Fu and Sheng (2009) presented a numerical model for simulation of the unsteady seepage flow through dam. These authors verified the reliability and accuracy of this model by laboratory data. A three-dimensional numerical manifold method for unconfined seepage analysis was proposed by Jiang et al. (2010). In this method, these researchers used tetrahedral finite element meshes. Bereslavskii (2011) simulated the plan steady state seepage in a homogeneous isotropic ground from channel as a hydrodynamic formulation. Alyavuz (2012) used a new computational analysis method known as discrete singular convolution (DSC) method for solving seepage flow problems. A numerical modeling was carried out for groundwater flow in Daxing, China, by Yang et al. (2012). Kazemzadeh-parsi and Daneshmand (2013) solved the 3D unconfined seepage problems using smoothed fixed grid finite element method. The transient seepage in an unsaturated porous media was solved by Pedroso (2015) using finite element solution. He also predicted the free surface location in the time-dependent problems. Athani

✉ Mahnaz Ghaeini-Hessaroeyeh
mghaeini@uk.ac.ir

1 Department of Civil Engineering, Faculty of Engineering, Shahid Bahonar University of Kerman, P.O. Box 76169133, Kerman, Iran

et al. (2015) presented the results of seepage and stability analysis of an earth dam using finite element method. A groundwater model was developed by Karay and Hajnal (2015) for flow in fractured rocks. These authors considered the non-laminar flow in discontinuities. Fukuchi (2016) studied the steady state seepage problems using interpolation finite difference method. He was able to solve two- and three-dimensional elliptic partial differential equations over the complicated domain. He also achieved results with high accuracy. The 2D subsurface seepage flow in an anisotropic porous medium was simulated by Lande et al. (2016). In this simulation, a new analytical solution was developed to estimate the transient behavior of the phreatic surface. Yuan and Zhong (2016) proposed a weak form quadrature element formulation in three-dimension for analysis of unconfined seepage in an earth dam. These authors validated the numerical solution by comparing with the available analytical and numerical solutions. Jiang et al. (2017) simulated the groundwater bypass seepage at the dam site of Dongzhiang hydro-junction. They considered Hydrological conditions include underground water divides, a hanging river and hydraulic drops along faults.

In this paper, it is developed a new finite element method for modeling the seepage problems. In this present approach, spherical Hankel shape functions are used instead of Lagrange shape functions in finite element method. Generally, in the classical FEM, when the number of elements are increased or in other words, when the mesh used is refined, the numerical solution become close to the exact solution, but by doing so, the CPU time and storage space are enhanced. Therefore, by using the new suggested shape functions, the degrees of freedom can be decreased while high accuracy can be resulted.

In order to estimate multivariable functions by linear combinations of terms depending on a univariate function, radial basis functions (RBFs) are used (Buhmann 2003). RBFs are categorized into two classes: oscillatory and non-oscillatory. The Gaussian functions, the thin plate splines, compact supported functions, multiquadrics and inverse multiquadrics are in the non-oscillatory class, while real and complex Fourier and J-Bessel RBFs are placed in oscillatory category (Hamzeh Javaran et al. 2011a, 2011b; Hamzehei Javaran and Khaji 2012, 2014; Khaji and Hamzehei Javaran 2013; Hamzehei Javaran and Shojaee 2017; Bahrampour et al. 2018; Farmani et al. 2018).

Complex Fourier and J-Bessel RBFs were proposed by Hamzeh Javaran et al. (2011a). The J-Bessel RBFs only have the properties of the first kind of Bessel function, while spherical Hankel shape functions contain the features of both first and second kind of Bessel functions, simultaneously. Therefore, this is the reason of the robustness of Hankel functions for increasing the solution accuracy. In the area

of the application of Hankel shape functions, Mousavi et al. (2021) solved fracture mechanics problem using boundary element method based on these functions recently.

In order to apply Hankel functions in the fluid mechanics, first, Farmani et al. (2018) made an improvement in the solution of Navier–Stokes equations for the benchmark fluid mechanics problems. Then, Hankel shape functions are used for boundary value problems (Farmani et al. 2019a) and for the sloshing behavior in 2-D tanks (Farmani et al. 2019b). Recently, Hankel shape functions are used for modeling the performance of Tuned Liquid Dampers (TLD) and also the interaction force between TLD-structure (Farmani et al. 2021). According to the past researches, it is useful to investigate the performance of the Hankel shape functions in the seepage and groundwater flow modeling in this paper.

The present paper consists of the following parts: at first, the governing equation and FEM formulation are stated. Then, spherical Hankel shape function and enrichment procedure are investigated. After that, to validate the proposed method for the leakage flows problems, one boundary value problem with different boundary conditions is solved and the results obtained are compared with the analytical solution. Also, in order to show applicability and reliability, five numerical problems are studied including saturated and unsaturated flow in porous media. Finally, the results are analyzed and the accuracy and precision of the present model are demonstrated.

Methods

The governing equations and FEM formulation are discussed in this part. Then, the suggested functions and the enrichment procedure are stated.

Governing equation and FEM formulation

In order to study the behavior of water in the porous media, two-dimensional seepage flow is considered. Therefore, the governing equation can be written as Eq. (1) which is obtained from Darcy's and continuity laws (Lam et al. 1987).

$$\frac{\partial}{\partial x}\left(k_x \frac{\partial h(x \cdot y \cdot t)}{\partial x}\right) + \frac{\partial}{\partial y}\left(k_y \frac{\partial h(x \cdot y \cdot t)}{\partial y}\right) = \rho_w g m_2^w \frac{\partial h(x \cdot y \cdot t)}{\partial t}$$
(1)

The above relation is a general equation that takes into account the transient condition. k_x and k_y are hydraulic permeability coefficients in x and y directions, respectively. $h(x \cdot y \cdot t)$ denote hydraulic head. Also, ρ_w and g indicate the density of water and gravitational acceleration, respectively. m_2^w is the slop of water retention curve.

There are two types of boundary conditions for seepage problems: boundary with specific head (Dirichlet

boundary condition) and impermeable boundary (Neumann boundary conditions) which are expressed as $h = h_0$ and $\partial h/\partial n$, respectively. Of course, for the groundwater problems, if there is a river in the aquifer domain, Neumann boundary conditions in the form of $\partial h/\partial n = q_0$, can be considered.

The purpose of numerical modeling is finding the unknown variable $h(x, y)$. Therefore, in the finite element method, the nodal variables are expressed by the following relation:

$$h(x, y) = \sum_{j=1}^{\widehat{m}} \psi_j(x, y)h_j \tag{2}$$

where ψ_j denotes the interpolation (shape) function. Using the FEM in solving Eq. (1), the below relation can be resulted:

$$\mathbf{M}\,\dot{\mathbf{h}}^{n'} + \mathbf{K}\,\mathbf{h}^{n'} = \tilde{\mathbf{F}} \tag{3}$$

According to employment of the four-node elements, it can be written as:

$$\mathbf{M} = \iint\limits_{A} (\tilde{m}\,\psi\psi^T)\,\mathrm{d}A$$

$$\mathbf{K} = \iint\limits_{A} \mathbf{BCB}^T\,\mathrm{d}A$$

$$\tilde{\mathbf{F}} = \iint\limits_{A} q\psi\,\mathrm{d}A \tag{4}$$

$$\mathbf{h}^{n'} = \begin{bmatrix} h_1 \\ h_2 \\ h_3 \\ h_4 \end{bmatrix}$$

$$\mathbf{B}^T = \begin{bmatrix} \frac{\partial \psi_1}{\partial x} & \frac{\partial \psi_2}{\partial x} & \frac{\partial \psi_3}{\partial x} & \frac{\partial \psi_4}{\partial x} \\ \frac{\partial \psi_1}{\partial y} & \frac{\partial \psi_2}{\partial y} & \frac{\partial \psi_3}{\partial y} & \frac{\partial \psi_4}{\partial y} \end{bmatrix}$$

$$\mathbf{C} = \begin{bmatrix} k_x & 0 \\ 0 & k_y \end{bmatrix}$$

in which $\tilde{m} = \rho_w g\, m_2^w$ and $\dot{\mathbf{h}}^{n'}$ is time derivative of nodal hydraulic head.

It should be noted that ψ can be classic Lagrange or Hankel shape functions. In the following section, the development procedure of Hankel functions is stated.

Suggested new shape functions

The J-Bessel functions that have been used in the other researches contain just the properties of the first kind of Bessel functions. Equation (5) expresses the Bessel equation of order u:

$$x^2 y'' + xy' + (x^2 - u^2)y = 0 \tag{5}$$

The solution of Eq. (5) is in the form of the following form:

$$y = AJ_u + BY_u \tag{6}$$

in which A and B are constant and J_u and Y_u show the first and second kind Bessel of order u, respectively. It should be noted that the first kind of Bessel functions is not capable of describing all properties of a physical phenomenon, while, by combining the first and second kind of it, Hankel RBFs are obtained and by using them, the numerical modeling is improved. In the following section, the enrichment process is stated completely.

Enrichment procedure of spherical Hankel shape functions

In this part, the enrichment procedure of Hankel RBFs is stated for an arbitrary n-node element in ξ direction, which is shown in Fig. 1.

At first, the polynomial terms and functional expansion of redial basis functions are combined:

$$w_h(\mathbf{x}) = \sum_{i=1}^{n} R_i(r)c_i + \sum_{j=1}^{m} P_j(\mathbf{x})d_j = \mathbf{R}^T(r)c + \mathbf{P}^T(\mathbf{x})d \tag{7}$$

in which n and m show the number of nodes and basis polynomial terms, respectively. Also, the following relation indicates the parameters and functions used in relation (7).

$$\begin{aligned} \mathbf{c}^T &= \begin{bmatrix} c_1 & c_2 & \dots & c_n \end{bmatrix}, \quad \mathbf{d}^T \\ &= \begin{bmatrix} d_1 & d_2 & \dots & d_m \end{bmatrix} \mathbf{R}^T(r) \\ &= [R_1(r) \quad R_2(r) \quad \dots \quad R_n(r)], \quad \mathbf{P}^T(\mathbf{x}) \\ &= [P_1(\mathbf{x}) \quad P_2(\mathbf{x}) \quad \dots \quad P_m(\mathbf{x})] \end{aligned} \tag{8}$$

If the nodal points are replaced in Eq. (7), relation (9) can be resulted:

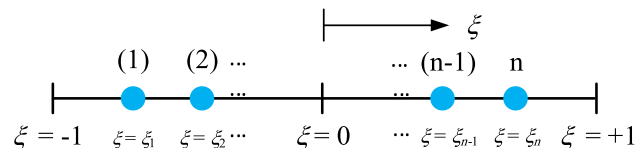$$\hat{\mathbf{w}} = \mathbf{R}_Q \mathbf{c} + \mathbf{P}_m \mathbf{d} \tag{9}$$

where

Fig. 1 The n-node element in one dimension

$$
\mathbf{R}_Q = \begin{bmatrix} R_1(r_1) & \cdots & R_n(r_1) \\ \cdot & & \cdot \\ \cdot & & \cdot \\ \cdot & & \cdot \\ R_1(r_n) & \cdots & R_n(r_n) \end{bmatrix}, \quad \mathbf{P}_m = \begin{bmatrix} P_1(\mathbf{x}_1) & \cdots & P_m(\mathbf{x}_1) \\ \cdot & & \cdot \\ \cdot & & \cdot \\ \cdot & & \cdot \\ P_1(\mathbf{x}_n) & \cdots & P_m(\mathbf{x}_n) \end{bmatrix} \tag{10}
$$

It should be noted that the number of unknowns in Eq. (9) is equal to $n + m$, while there are only n equations, and thus in order to balance the number of knowns and unknowns, additional conditions are essential [for more details see Farmani et al. (2018) and Bahrampour et al. (2018)].

Finally, the set of equations can be resulted as the following form:

$$
\begin{bmatrix} \mathbf{R}_Q & \mathbf{P}_m \\ \mathbf{P}_m^T & 0 \end{bmatrix} \begin{bmatrix} \mathbf{c} \\ \mathbf{d} \end{bmatrix} = \begin{bmatrix} \hat{\mathbf{w}} \\ 0 \end{bmatrix} \tag{11}
$$

By using some algebraic manipulations, relation (12) is resulted:

$$
\mathbf{c} = \mathbf{S}_c \hat{\mathbf{w}}, \quad \mathbf{d} = \mathbf{S}_d \hat{\mathbf{w}} \tag{12}
$$

in which,

$$
\mathbf{S}_c = \mathbf{R}_Q^{-1} - \mathbf{R}_Q^{-1} \mathbf{P}_m \mathbf{S}_d, \quad \mathbf{S}_d = [\mathbf{P}_m^T \mathbf{R}_Q^{-1} \mathbf{P}_m]^{-1} \mathbf{P}_m^T \mathbf{R}_Q^{-1} \tag{13}
$$

If $\mathbf{c}$ and $\mathbf{d}$ are replaced into Eq. (7), the following relation can be obtained:

$$
w_h(\mathbf{x}) = [\mathbf{R}^T(r)\mathbf{S}_c + \mathbf{P}^T(\mathbf{x})\mathbf{S}_d]\hat{\mathbf{w}} \tag{14}
$$

The final matrix of the shape functions is suggested as below:

$$
\boldsymbol{\Psi}(\mathbf{x}) = \mathbf{R}^T(r)\mathbf{S}_c + \mathbf{P}^T(\mathbf{x})\mathbf{S}_d \tag{15}
$$

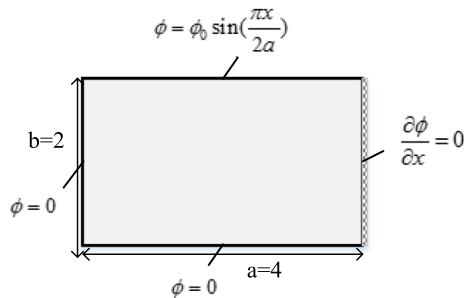Consequently, the following relation expresses the intended RBF:

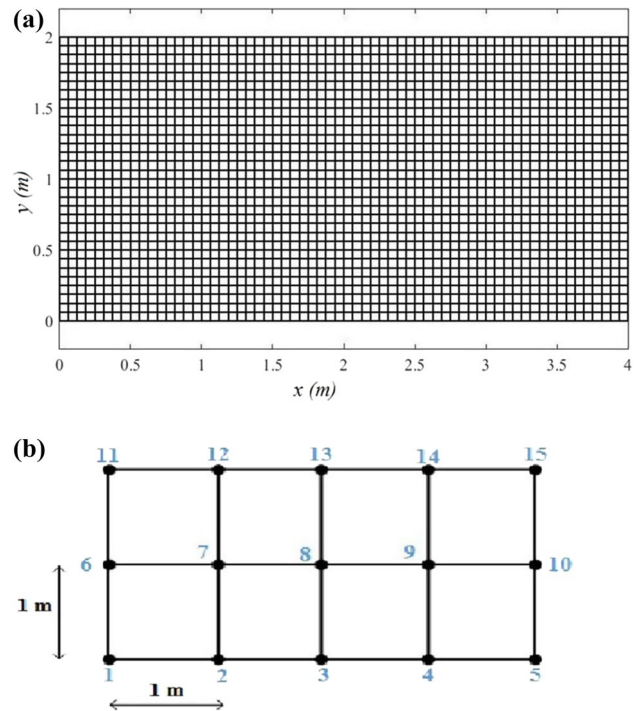**Fig. 2** Domain and different boundary conditions for validation problem

Fig. 3 Meshed domain with **a** 2048 elements, **b** 8-element with nodes number for validation problem

$$
R(r) = (\varepsilon r)^{\tilde{n}+1} h_{\tilde{n}}^{(1)}(\varepsilon r), \quad \varepsilon > 0, \quad \tilde{n} = 0, 1, 2, \ldots \tag{16}
$$

that ε and $\tilde{n}$ denote the shape parameters of Hankel RBF and $h_{\tilde{n}}^{(1)}(\varepsilon r) = \sqrt{\frac{\pi}{2(\varepsilon r)}} H_{\tilde{n}+\frac{1}{2}}^{(1)}(\varepsilon r)$ shows the spherical Hankel function of the first kind.

Since there is a singularity at imaginary part of $h_{\tilde{n}}^{(1)}(\varepsilon r) = j_{\tilde{n}}(\varepsilon r) + i y_{\tilde{n}}(\varepsilon r)$, the term of $(\varepsilon r)^{\tilde{n}+1}$ is applied for resolving this problem. Thus the limiting values of the RBF can be obtained as:

$$
\lim_{r \to 0} (\varepsilon r)^{\tilde{n}+1} h_{\tilde{n}}^{(1)}(\varepsilon r) = 0 + \frac{(-1)^{\tilde{n}+1} 2^{\tilde{n}} \sqrt{\pi}}{\Gamma(-\tilde{n} + \frac{1}{2})} i \tag{17}
$$

The intended RBF for n-node element shown in Fig. 1 is calculated as below:

$$
\mathbf{R}(r) = \begin{bmatrix} R_1(r) \\ R_2(r) \\ \cdot \\ \cdot \\ \cdot \\ R_n(r) \end{bmatrix} = \begin{bmatrix} (\varepsilon|\xi - \xi_1|)^{\tilde{n}+1} g_{\tilde{n}}^{(1)}(\varepsilon|\xi - \xi_1|) \\ (\varepsilon|\xi - \xi_2|)^{\tilde{n}+1} h_{\tilde{n}}^{(1)}(\varepsilon|\xi - \xi_2|) \\ \cdot \\ \cdot \\ \cdot \\ (\varepsilon|\xi - \xi_n|)^{\tilde{n}+1} h_{\tilde{n}}^{(1)}(\varepsilon|\xi - \xi_n|) \end{bmatrix} \tag{18}
$$

In the enrichment process of Hankel RBF, the matrices can be expressed as:

Table 1 Comparison of the results among Hankel shape function (8 elements), Lagrange shape function (8 and 2048 elements) and analytical solution for validation problem

Node	Lagrange shape function (8 elements) (relative error%)	Hankel shape function (8 elements) (relative error%)	Solution with 2048 elements (relative error%)	Analytical solution
7	0.259 (2.99)	0.265 (0.75)	0.267 (0)	0.267
8	0.370 (1.85)	0.375 (0.53)	0.377 (0)	0.377
9	0.291 (8.98)	0.270 (1.12)	0.267 (0)	0.267
10	0.249 (–)	0.06 (–)	0 (–)	0
	L^2 relative error norm $=46.92\%$	L^2 relative error norm $=11.27\%$	L^2 relative error norm $=0\%$	
	Computational time $=1.57$ s	Computational time $=1.91$ s	Computational time $=2.52$ s	
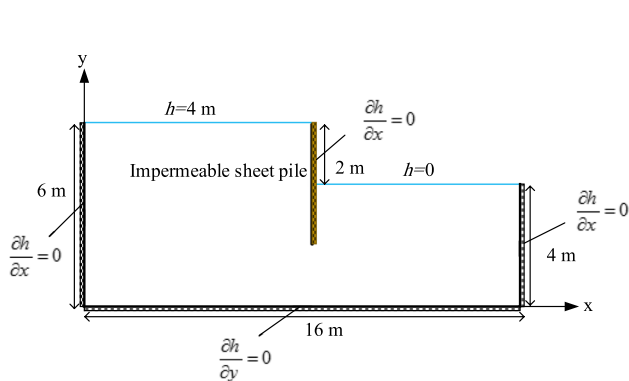
Fig. 4 Computational domain and boundary conditions for the first problem

$$\mathbf{P}(\xi) = \begin{bmatrix} 1 \\ \xi \\ \cdot \\ \cdot \\ \cdot \\ \xi^{n-2} \end{bmatrix} \tag{19}$$

$$\mathbf{R}_Q =$$

$$\begin{bmatrix} \beta & (\epsilon|\xi_1 - \xi_2|)^{\bar{n}+1} h_{\bar{n}}^{(1)}(\epsilon|\xi_1 - \xi_2|) & \cdot & \cdot & \cdot & (\epsilon|\xi_1 - \xi_n|)^{\bar{n}+1} h_{\bar{n}}^{(1)}(\epsilon|\xi_1 - \xi_n|) \\ & \cdot & & & & (\epsilon|\xi_2 - \xi_n|)^{\bar{n}+1} h_{\bar{n}}^{(1)}(\epsilon|\xi_2 - \xi_n|) \\ & & & & & \cdot \\ & \text{sym.} & & \cdot & & \cdot \\ & & & & \cdot & \cdot \\ & & & & & \beta \end{bmatrix}$$

$$\tag{20}$$

Fig. 5 Meshed domain with **a** 1280 elements, **b** 10-element for the first problem
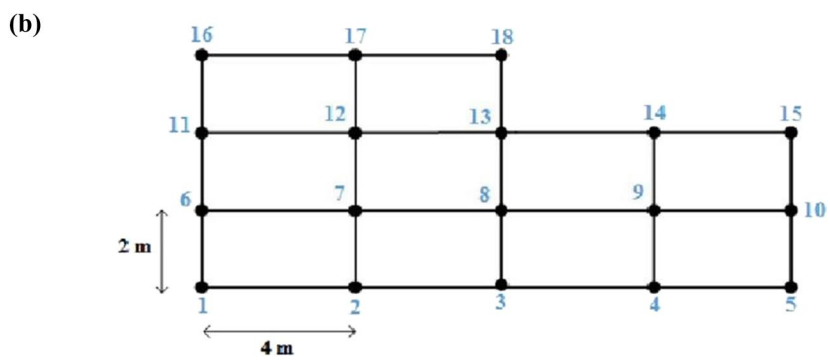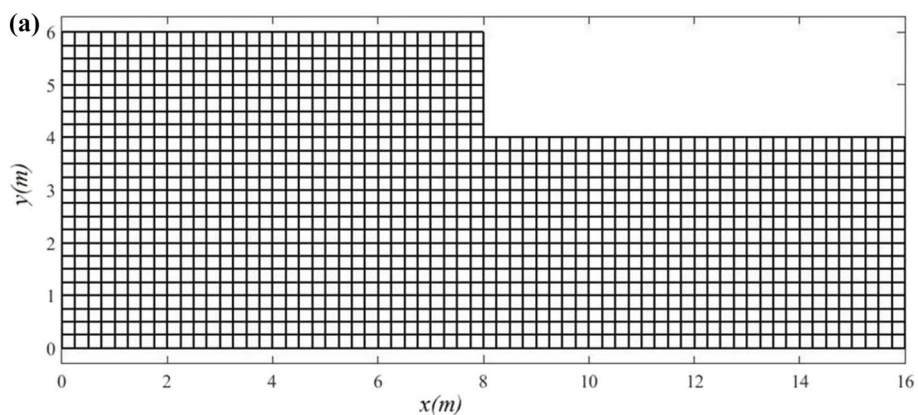
Table 2 Comparison of the results among Hankel shape function (10 elements) and Lagrange shape function (10 and 1280 elements) for the first problem

Node	Lagrange shape function (10 elements) (relative error%)	Hankel shape function (10 elements) (relative error%)	Solution with 1280 elements
1	3.110 (1.70)	3.151 (0.41)	3.164
2	2.449 (9.23)	2.569 (4.78)	2.698
3	1.01 (23.19)	1.221 (7.15)	1.315
4	0.194 (42.09)	0.284 (15.22)	0.335
5	0.0466 (65.22)	0.114 (14.92)	0.134
6	3.274 (0.03)	3.273 (0)	3.273
7	2.616 (7.79)	2.725 (3.95)	2.837
8	0.846 (30.71)	0.919 (24.73)	1.221
9	0.111 (53.94)	0.226 (6.22)	0.241
10	0.0426 (55.48)	0.0875 (8.57)	0.0957
11	3.504 (2.040)	3.552 (0.7)	3.577
12	3.480 (5.87)	3.316 (0.88)	3.287
	L^2 relative error norm $= 8.326\%$	L^2 relative error norm $= 4.61\%$	
	Computational time $= 1.27$ s	Computational time $= 1.5$ s	Computational time $= 2.1$ s
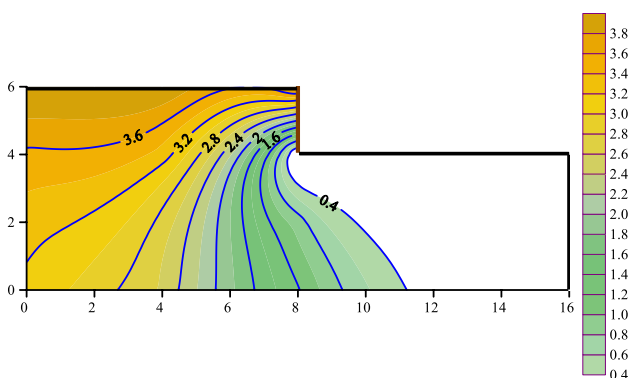
Fig. 6 Contours of hydraulic head (m) for the first problem with 18 nodes
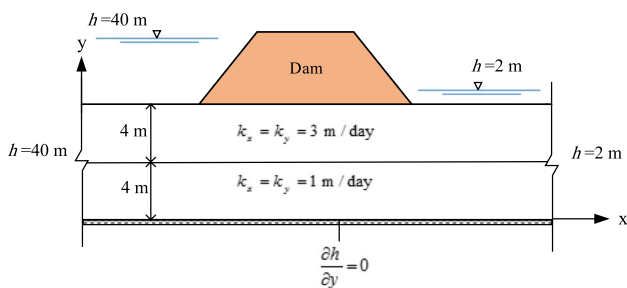
Fig. 7 Computational domain and boundary conditions for the second problem

$$\mathbf{P}_m = \begin{bmatrix} 1 & \xi_1 & . & . & . & \xi_1^{n-2} \\ 1 & \xi_2 & . & . & . & \xi_2^{n-2} \\ . & . & . & & & . \\ . & . & . & & & . \\ . & . & . & & & . \\ 1 & \xi_n & . & . & . & \xi_n^{n-2} \end{bmatrix} \qquad (21)$$

where, $\beta = \lim_{r \to 0} R(r)$, which is restricted by deleting the singularity in Eq. (17).

Finally, the shape functions for an n-node element are written as relation (22):

$$\mathbf{\Psi}(\xi) = \begin{bmatrix} \psi_1(\xi) & \psi_2(\xi) & . . . & \psi_n(\xi) \end{bmatrix}$$
$$\psi_m = \frac{FG - E}{(FG - E)\big|_{\xi = \xi_m}} \qquad m = 1, 2, ..., n \qquad (22)$$

where F, G and E are expressed as:

$$F = F(\xi_1, \xi_2, ..., \xi_{m-1}, \xi_{m+1}, ..., \xi_n) = \prod_{\substack{j < o \\ j, o \neq m}} (\xi_j - \xi_o) \qquad (23)$$

$$G = G(\xi; \xi_1, \xi_2, ...\xi_n)$$
$$= \sum_{k \in A} \left\{ (-1)^k \prod_{\substack{j < o \\ j, o \neq k}} \{(\xi_j - \xi_o)\}(\varepsilon|\xi - \xi_k|)^{\tilde{n}+1} h_{\tilde{n}}^{(1)}(\varepsilon|\xi - \xi_k|) \right\} \qquad (24)$$

$$E = \sum_{j \neq m} F\big|_{\xi_j = \xi} G\big|_{\xi_j = \xi} \qquad (25)$$

that $j, o \in A$ and the set A is expressed as $A = \{1, 2, ..., n\}$ (Farmani et al. 2018).

It should be noted that the spherical Hankel shape functions have some properties such as Kronecker delta property, Partition of unity, Linear independence property and Infinite piecewise continuity which are stated completely in Farmani et al. (2018) and Bahrampour et al. (2018).

The above process can be easily extended to 2-D elements. In this paper, four-node quadrilateral elements are used for solving the seepage problems by the classic finite element and new methods.

Fig. 8 Meshed domain with **a** 3072 elements, **b** 12 elements for the second problem
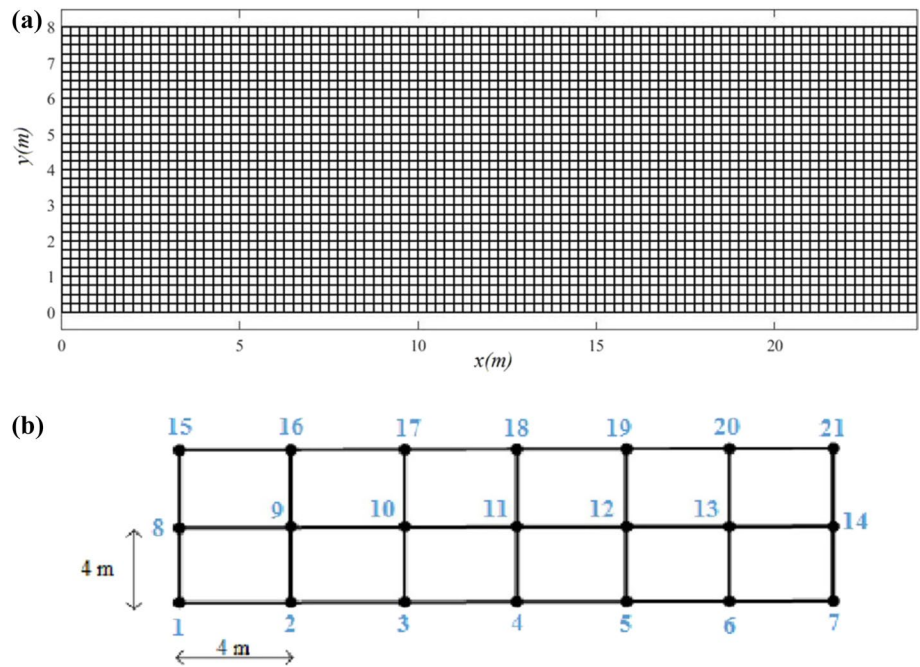

Table 3 Comparison of the results among Hankel shape function (12 elements) and Lagrange shape function (12 and 3072 elements) for the second problem

Node	Lagrange shape function (12 elements) (relative error%)	Hankel shape function (12 elements) (relative error%)	Solution with 3072 elements
2	34.742 (1.22)	34.998 (0.49)	35.173
3	28.408 (1.16	28.554 (0.65)	28.742
4	21.0 (1.93)	21.321 (0.43)	21.414
5	13.591 (3.35)	13.954 (0.77)	14.062
6	7.257 (2.55)	7.384 (0.84)	7.447
9	35.548 (1.99)	35.986 (0.79)	36.273
10	29.215 (0.271)	29.141 (0.017)	29.136
11	21.0 (1.97)	21.320 (0.47)	21.422
12	12.784 (6.77)	13.516 (1.43)	13.713
13	6.451 (2.89)	6.613 (0.45)	6.643
17	29.066 (0.998)	29.215 (0.49)	29.359
18	21.0 (1.97)	21.320 (0.48)	21.423
19	12.934 (4.093)	13.257 (1.69)	13.486
	L^2 relative error norm $=2.01\%$	L^2 relative error norm $=0.655\%$	
	Computational time $=1.29$ s	Computational time $=1.82$ s	Computational time $=3.6$ s

Results and discussion

Validation

In this section, to validate and verify the numerical modeling of leakage problems, Laplace equation $(\partial^2\phi/\partial x^2 + \partial^2\phi/\partial y^2 = 0)$ is solved for the domain shown in Fig. 2. In this problem, both boundary conditions, namely Dirichlet and Neumann conditions, exist. Thus, it can be a suitable representative for the seepage flow problems. For

the modeling, the numerical results are obtained with high number of elements and then 8 elements for both methods (Fig. 3). Then, these results are compared with the analytical solution [Eq. (26)] and presented in Table 1.

$$\phi(x, y) = \frac{\phi_0}{\sinh\left(\frac{\pi b}{a}\right)} \sin\left(\frac{\pi x}{a}\right) \sinh\left(\frac{\pi y}{a}\right) \qquad (26)$$

According to the results in Table 1, it can be justified that firstly, Hankel shape functions with 8 elements present
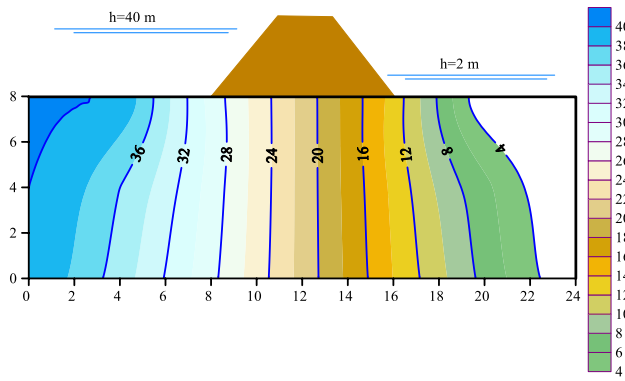
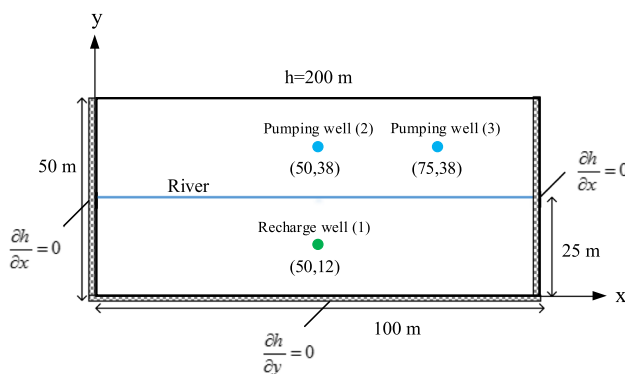**Fig. 9** Contours of hydraulic head (m) for the second problem with 21 nodes

Fig. 10 Computational domain and boundary conditions for the third problem

more accurate results than Lagrange shape functions with the same mesh. Secondly, Lagrange functions with high number of elements have very good agreement with the analytical solution. Thus the model with high degrees of freedom can be selected as a comparison source for the study of applicability and efficiency of the proposed approach for the seepage problems.

Applicability

In order to demonstrate the applicability and robustness of the suggested formulation in the seepage flows, various numerical models are carried out. Then the present model results with coarse meshes are compared with the traditional FEM with the same and refined meshes. The results are presented in the framework of tables and graphs. It should be noted that, for the results in the tables, the relative error L^2 relative error norm and the computational time are presented.

First problem: groundwater flow under a coffer dam

The first problem is the steady state groundwater flow beneath a coffer dam. The computational domain with boundary conditions is shown in Fig. 4 (Reddy 2004). The Laplace equation is solved by the present model and also the classic method. For this purpose, a coarse mesh (10 elements) and then a mesh with high number of elements are chosen (Fig. 5). The results obtained from both methods are given in Table 2.

According to the Table 2, it is inferred that with fewer number of elements in the present formulation, better accuracy than the classic FEM is achieved and the calculated errors are also less. Also, the contours of hydraulic head are indicated in Fig. 6 for this problem with 10-element mesh.

Second problem: flow through the foundation of a dam

In this case, the steady state seepage flow of soil foundation of a dam is studied. It is assumed that the soil under the dam is isotropic and heterogeneous (Reddy 2004). Figure 7 displays the geometry and boundary conditions for this problem. The governing equation is solved by both methods with refined meshes and then the meshes with low number of elements. The grids are shown in Fig. 8. To compare the proposed method results with the classic finite element method, the results are indicated in Table 3. The errors are also computed based on the numerical solution with high degrees of freedom.

As it can be observed in Table 3, the proposed formulation has better agreement with the results by high elements compared with the classic method with the same number of elements. For this case, Fig. 9 shows the contours of hydraulic head for the mesh with 12 elements.

Third problem: groundwater flow in an aquifer with river boundary, pumping and recharges wells

In this part, a homogeneous and anisotropic aquifer is investigated. Equation (1) with steady state condition is solved using the proposed and classical methods. For this problem, the permeability coefficients are considered $k_x = 1.75$ m/day and $k_y = 1$ m/day in the x and y-direction, respectively. Furthermore, it is assumed that a river passes through the aquifer with infiltrating rate of $q_0 = 0.5$ m^3/day/m. Two pumping wells and one recharges well with rates of $Q_1 = 900$ m^3/day, $Q_2 = -220$ m^3/day and $Q_3 = -450$ m^3/day are also considered (Reddy 2004). The geometry, boundary conditions, the locations of river and wells are illustrated in Fig. 10. The grids with 100×50 and 4×4 meshes are used which are depicted in Fig. 11. Also, Figs. 12 and 13 show the results obtained from the both methods at $y = 0$ and $y =$

Fig. 11 Meshed domain with **a** 5000 elements, **b** 16 elements for the third problem
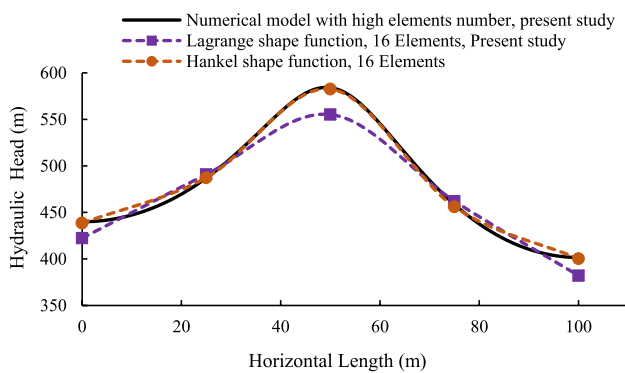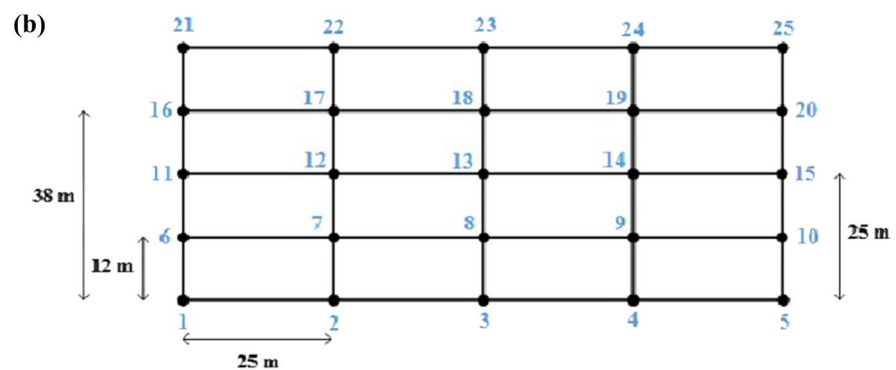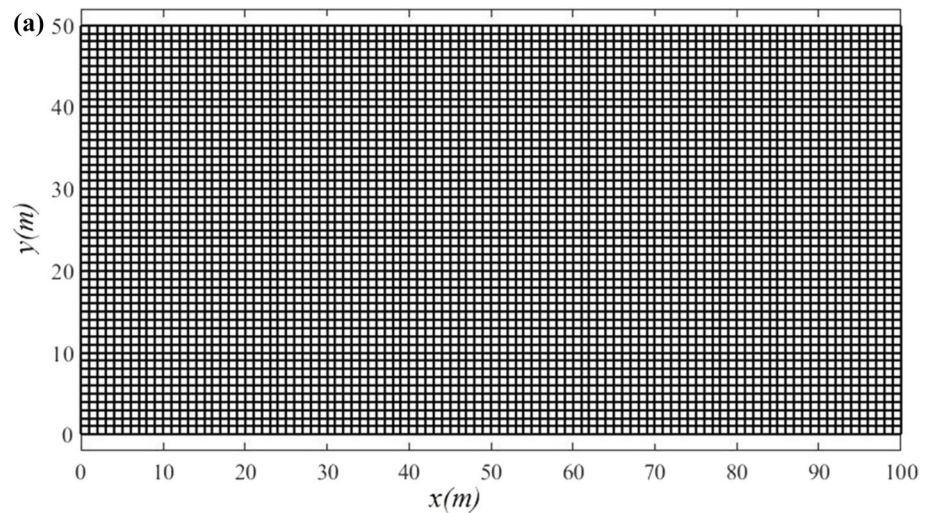

Fig. 12 Comparison of hydraulic head results at $y = 0$, among Hankel shape function (16 elements) and Lagrange shape function (16 and 5000 elements) for the third problem
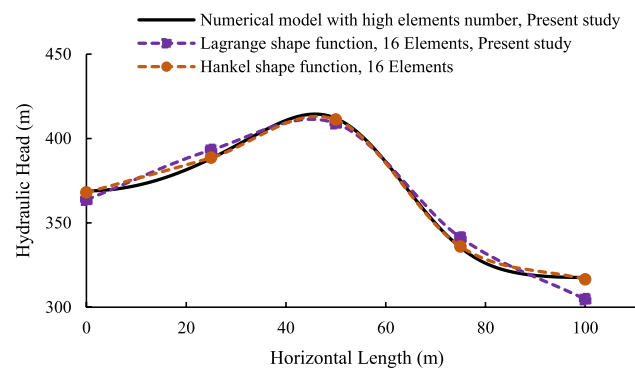

Fig. 13 Comparison of hydraulic head results at $y = 25$ m, among Hankel shape function (16 elements) and Lagrange shape function (16 and 5000 elements) for the third problem

25 m, respectively. The contours of head are also given in Fig. 14 for the 16-element mesh. It should be noted that the computational time of this problem for Hankel and Lagrange functions with 16 elements and Lagrange functions with 5000 elements is 2.11, 1.7 and 11.1 s, respectively.

According to Figs. 11 and 12, it can be found that using spherical Hankel shape functions with 16 elements leads to

having better results than Lagrange shape functions with the same mesh.

Fourth problem: groundwater flow in anisotropic heterogeneous region with river boundary

A domain with different permeability in two directions is considered in this section. Then, the steady state
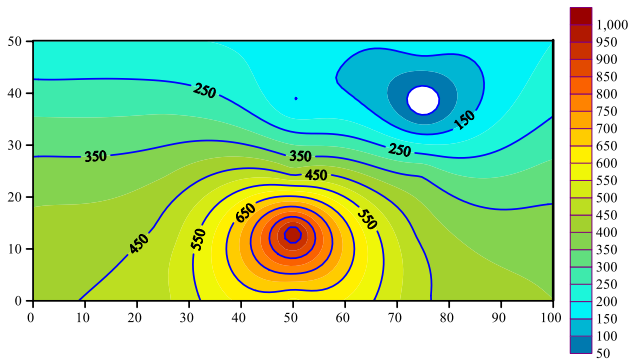
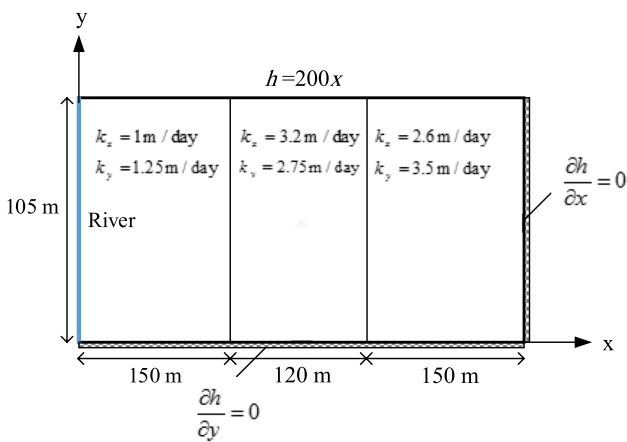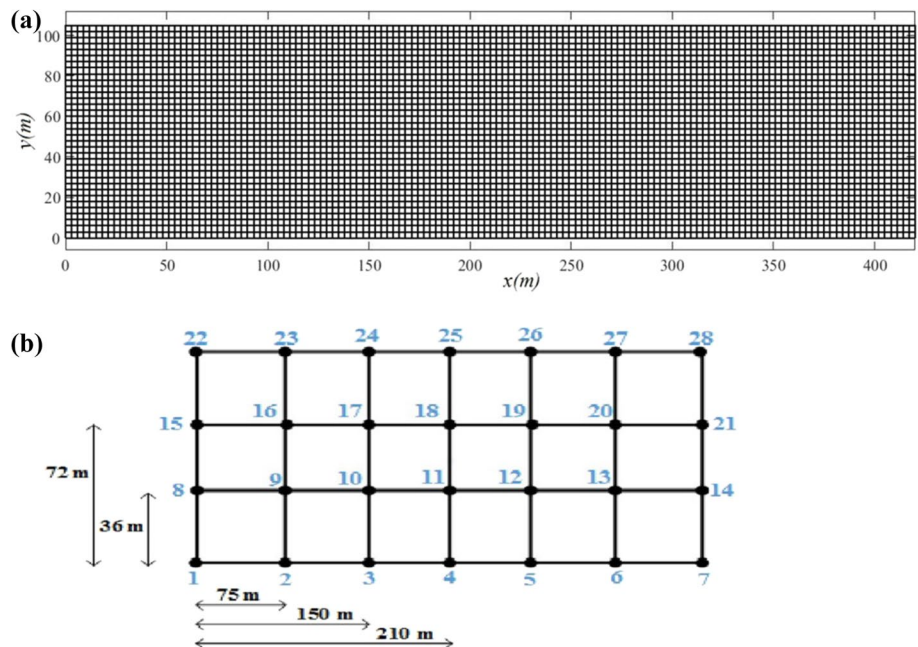**Fig. 14** Contours of hydraulic head (m) for the third problem with 25 nodes

Fig. 15 Computational domain and boundary conditions for the fourth problem

Fig. 16 Meshed domain with **a** 4900 elements, **b** 18 elements for the fourth problem

groundwater flow is studied for the intended aquifer. In the top boundary, the hydraulic head is varied as linear and in the function of x. There is a river at the left boundary with rate of $q_0 = 0.24$ m^3/day/m. Other boundaries are impermeable (Reddy 2004). The computational domain and boundary conditions are also shown in Fig. 15. Also, the meshes used are illustrated in Fig. 16. The numerical results are also exhibited in Fig. 17 and Table 4. The contours of hydraulic head are presented in Fig. 18.

It can be concluded from Fig. 17 and Table 4 that the suggested formulation improves the accuracy in the numerical modeling of the mentioned problem. The computational time of Hankel functions is marginally more than Lagrange functions with the same mesh for all problems. However, this time is less than Lagrange functions with high number of elements. Also, the improved accuracy using Hankel functions is significant.

Fifth problem: unsaturated–saturated soil with transient condition

A time-dependent seepage problem is investigated in this section. The studied soil consists of two unsaturated and saturated regions. In order to model the unsaturated part, the permeability coefficient (or hydraulic conductivity coefficient) is assumed to be a function of pore-water pressure. The permeability function for different soils is shown in Fig. 19.

The governing equation for seepage in unsaturated–saturated soil with transient condition is expressed as the following relation:
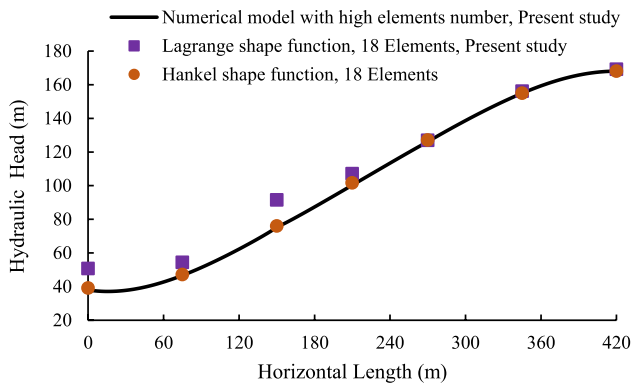
Fig. 17 Comparison of hydraulic head results at $y = 0$, among Hankel shape function (18 elements) and Lagrange shape function (18 and 4900 elements) for the fourth problem
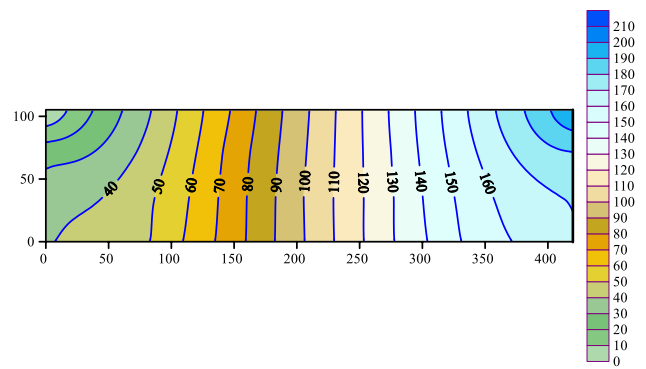

Fig.18 Contours of hydraulic head (m) for the fourth problem with 28 nodes

$$\frac{\partial}{\partial x}\left(k_{xx}\frac{\partial h(x \cdot y \cdot t)}{\partial x} + k_{xy}\frac{\partial h(x \cdot y \cdot t)}{\partial y}\right)$$
$$+ \frac{\partial}{\partial y}\left(k_{yx}\frac{\partial h(x \cdot y \cdot t)}{\partial x} + k_{yy}\frac{\partial h(x \cdot y \cdot t)}{\partial y}\right) \quad (27)$$
$$= \rho_w g m_2^w \frac{\partial h(x \cdot y \cdot t)}{\partial t}$$

In this paper, m_2^w value (the slop of water retention curve) is considered constant and equal to 0.0001 m²/kN. Figure 20 shows the water retention curve for this problem. It should be noted that the soil is assumed sandy for this problem. There is the anisotropic condition in the unsaturated part where the angle between the major permeability coefficient and x-axis is considered $\alpha = 30°$. In Eq. (27),
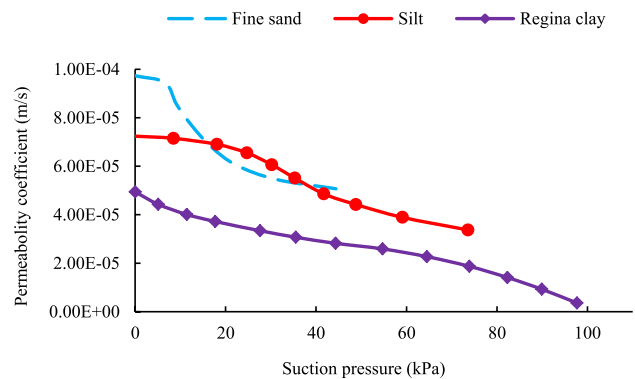

Fig. 19 Unsaturated permeability function for different soils (Lam et al, 1987)

Table 4 Comparison of the results among Hankel shape function (18 elements) and Lagrange shape function (18 and 4900 elements) for the fourth problem

| Node	Lagrange shape function (18 elements) (relative error%)	Hankel shape function (18 elements) (relative error%)	Solution with 4900 elements
8	45.962 (18.32)	37.003 (4.74)	38.844
9	51.380 (13.51)	46.665 (3.097)	45.263
10	89.758 (21.19)	75.656 (2.15)	74.062
11	106.075 (5.81)	102.056 (1.80)	100.250
12	126.945 (0.248)	126.790 (0.12)	126.631
13	157.433 (0.79)	156.554 (0.23)	156.199
14	171.935 (0.76)	170.947 (0.18)	170.638
15	30.378 (23.76)	25.585 (4.23)	24.545
16	43.253 (5.24)	40.850 (0.60)	41.097
17	83.905 (15.20)	74.458 (2.23)	72.831
18	103.242 (3.1)	101.016 (0.88)	100.132
19	127.195 (0.25)	127.651 (0.10)	127.514
20	161.060 (0.82)	160.756 (0.63)	159.745
21	181.423 (1.13)	180.030 (0.35)	179.394
	L^2 relative error norm = 5.51%	L^2 relative error norm = 0.98%	
	Computational time = 1.54 s	Computational time = 2.1 s	Computational time = 7.6 s
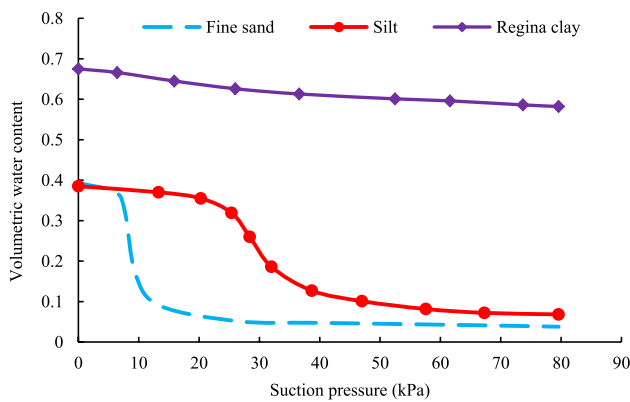
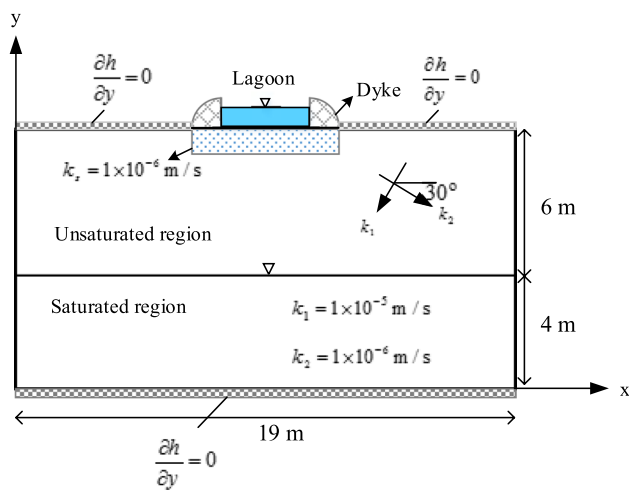**Fig. 20** Water retention curve for different soils (Lam et al, [1987])

Fig. 21 Computational domain and boundary conditions for the fifth problem
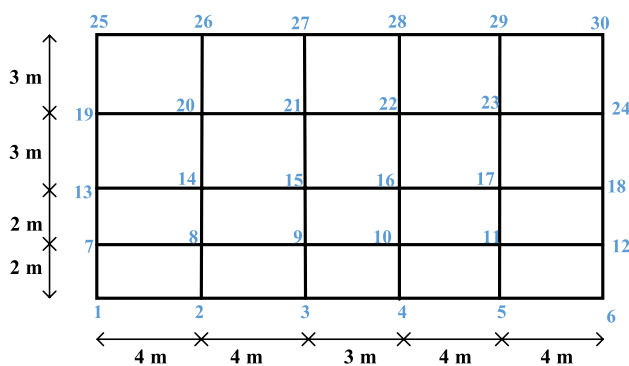

Fig. 22 Meshed domain with 20 elements for the fifth problem

$k_{xx} = k_1 \cos^2 \alpha + k_2 \sin^2 \alpha$, $k_{yy} = k_1 \sin^2 \alpha + k_2 \cos^2 \alpha$ and $k_{xy} = k_{yx} = (k_1 - k_2) \sin \alpha \cos \alpha$. That, k_1 and k_2 are the major and minor permeability coefficient, respectively.

It can be mentioned that matrix $\mathbf{C}$ is defined as $\mathbf{C} = \begin{bmatrix} k_{xx} & k_{xy} \\ k_{yx} & k_{yy} \end{bmatrix}$ for this problem.

In order to approximate the hydraulic head at the different time step, the central finite difference approximation is used as the following relation:

$$\left(\mathbf{K} + \frac{2\mathbf{M}}{\Delta t} \right) \mathbf{h}_{t+\Delta t}^{n'} = \left(\frac{2\mathbf{M}}{\Delta t} - \mathbf{K} \right) \mathbf{h}_t^{n'} - 2\tilde{\mathbf{F}} \tag{28}$$

where Δt is the time step that is considered equal to 0.5 min.

It should be noted that the transient seepage equation in the unsaturated region is nonlinear. Because the permeability coefficient is a function of pore-water pressure, an iterative scheme is needed to obtain the correct nodal hydraulic heads. First, an initial permeability is assumed and nodal heads are calculated. Then, the water-pore pressure is obtained by $(u_w)_t = \left(h_t^{n'} - z^{n'} \right) \rho_w g$ that $z^{n'}$ indicates the elevation at the nodes of the elements. Therefore, using the pressure and permeability function, a modified permeability value is considered to calculate the new nodal heads. This process is repeated until the difference of the head and permeability for two iterations are smaller than 0.0001.

To model this numerical example, the geometry with boundary conditions is considered according to illustrated conditions in Fig. 21. The problem discussed here is a transient groundwater flow in two unsaturated–saturated regions. The initial depth of water in pond is assumed 1 m. Also, a lining with permeability coefficient equal to 1×10^{-6} m/s is considered on the bottom of pond. At the left and right boundaries, there are hydrostatic conditions.

In order to investigate the applicability of this problem, the present model results are compared with the results of Lam et al. ([1987]). A grid with 20 elements (Fig. 22) is studied for the numerical modeling. Tables 5, 6, 7 and 8 present the nodal hydraulic head at different times using finite element method based on both Lagrange and Hankel functions. The negative sign for some values in the tables represents the suction pressure. Also, the contours of hydraulic head at the points when the time is equal to 1316 min are shown in Fig. 23 using 20 elements based on the proposed functions.

It is observed that Hankel functions present the results with more precision than Lagrange functions in comparison with numerical results of Lam et al. ([1987]). Although the computational cost of Hankel functions is slightly more, the increased accuracy is significant.

Conclusion

Leakage flow in soil was studied numerically by suggesting new shape functions based on the finite element method. In the proposed formulation, the new functions

Table 5 Comparison of the results obtained from Hankel shape function, Lagrange shape function and numerical solution of Lam et al. (1987) at $t = 22.5$ min for the fifth problem

Node	Lagrange shape function (20 elements) (relative error%)	Hankel shape function (20 elements) (relative error%)	Numerical modeling of Lam et al. (1987)
8	2.00 (0.00)	2.00 (0.00)	2.00
9	2.13 (6.50)	2.00 (0.00)	2.00
10	2.06 (3.00)	2.00 (0.00)	2.00
11	2.00 (0.00)	2.00 (0.00)	2.00
14	0.00 (–)	0.00 (–)	0.00
15	0.00 (–)	0.00 (–)	0.00
16	− 0.11 (–)	0.00 (–)	0.00
17	0.00 (–)	0.00 (–)	0.00
20	− 3.16 (5.33)	− 3.12 (4.00)	− 3.00
21	− 3.35 (8.06)	− 3.15 (1.61)	− 3.10
22	− 3.21 (7.00)	− 3.12 (4.00)	− 3.00
23	− 3.16 (5.33)	− 3.07 (2.33)	− 3.00
	L^2 relative error norm$=6.01\%$	L^2 relative error norm$=2.62\%$	

Table 6 Comparison of the results obtained from Hankel shape function, Lagrange shape function and numerical solution of Lam et al. (1987) at $t = 66.5$ min for the fifth problem

Node	Lagrange shape function (20 Elements) (Relative error%)	Hankel shape function (20 Elements) (Relative error%)	Numerical modeling of Lam et al. (1987)
8	2.10 (5.0)	2.0 (0.0)	2.0
9	2.11 (5.50)	2.0 (0.0)	2.0
10	2.20 (10.0)	2.13 (6.50)	2.0
11	2.10 (5.0)	2.0 (0.0)	2.0
14	− 0.09 (–)	0.0 (–)	0.0
15	− 0.15 (–)	− 0.12 (–)	0.0
16	− 0.09 (–)	0.0 (–-)	0.0
17	− 0.13 (30.0)	− 0.11 (10.0)	− 0.10
20	− 3.41 (13.66)	− 3.22 (7.33)	− 3.0
21	− 2.50 (7.40)	− 2.51 (7.03)	− 2.70
22	− 1.80 (5.88)	− 1.77 (4.11)	− 1.70
23	− 2.61 (16.0)	− 2.65 (6.0)	− 2.5
	L^2 relative error norm$=9.08\%$	L^2 relative error norm$=- 5.88\%$	

Table 7 Comparison of the results obtained from Hankel shape function, Lagrange shape function and numerical solution of Lam et al. (1987) at $t = 174$ min for the fifth problem

Node	Lagrange shape function (20 elements) (relative error%)	Hankel shape function (20 elements) (relative error%)	Numerical modeling of Lam et al. (1987)
8	2.23 (11.50)	2.10 (5.00)	2.00
9	2.20 (10.00)	2.11 (5.50)	2.00
10	2.25 (2.27)	2.10 (4.54)	2.20
11	2.44 (6.08)	2.35 (2.17)	2.30
14	0.11 (–)	0.10 (–)	0.00
15	0.15 (50.00)	0.12 (20.00)	0.10
16	0.62 (55.00)	0.50 (25.00)	0.40
17	0.50 (16.67)	0.55 (8.33)	0.60
20	− 2.74 (5.51)	− 2.82 (2.75)	− 2.90
21	− 1.55 (18.42)	− 1.66 (12.63)	− 1.90
22	− 1.20 (20.00)	− 1.14 (14.00)	− 1.00
23	− 1.29 (10.25)	− 1.22 (4.27)	− 1.17
	L^2 relative error norm$=10.87\%$	L^2 relative error norm$=6.59\%$	

Table 8 Comparison of the results obtained from Hankel shape function, Lagrange shape function and numerical solution of Lam et al. (1987) at $t = 1316$ min for the fifth problem

Node	Lagrange shape function (20 elements) (relative error%)	Hankel shape function (20 elements) (relative error%)	Numerical modeling of Lam et al. (1987)
8	2.41 (9.54)	2.30 (4.54)	2.20
9	2.64 (5.60)	2.45 (2.00)	2.50
10	2.86 (5.93)	2.60 (3.70)	2.70
11	2.78 (6.93)	2.70 (3.84)	2.60
14	0.71 (42.00)	0.60 (20.00)	0.50
15	0.95 (18.75)	0.88 (10.00)	0.80
16	1.37 (37.00)	1.26 (26.00)	1.00
17	0.70 (22.22)	1.00 (11.11)	0.90
20	− 2.72 (4.61)	− 2.70 (3.85)	− 2.60
21	− 1.40 (6.67)	− 1.43 (4.67)	− 1.50
22	− 0.98 (40)	− 0.85 (21.43)	− 0.70
23	− 1.50 (15.38)	− 1.41 (8.46)	− 1.30
	L^2 relative error norm $= 11.41\%$	L^2 relative error norm $= 6.71\%$	
	Computational time $= 4620.12$ s	Computational time $= 4627.2$ s	

were derived by combining polynomials and spherical Hankel radial basis functions, and therefore, they contain the advantages of both functions. These advantages also provide robustness and strength for the offered approach. In addition, these properties improve the solution accuracy with fewer degrees of freedom. In order to validate the present method, one boundary value problem with different boundary conditions was studied and then the results were compared with analytical solution. Also, five seepage numerical problems for finding hydraulic head were investigated, and through them, the applicability and reliability of the proposed method were examined. The results indicated that the present model with the low number of elements is more efficient than the classic FEM with the same mesh.

Fig. 23 Contours of hydraulic head (m) for the fifth problem with 30 nodes

Declarations

References

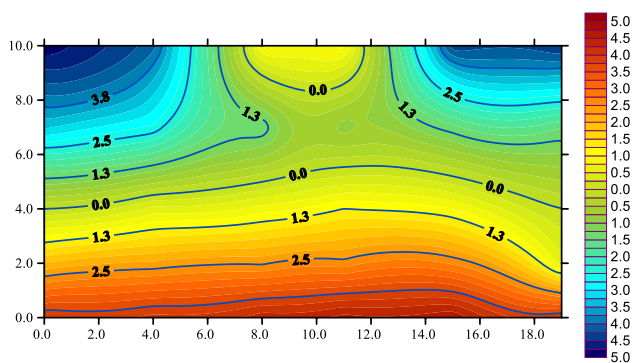Alyavuz B (2012) Numerical solution of 2d seepage flow problem using discrete singular convolution method. Int J Numer Meth Heat Fluid 22(5):607–621. https://doi.org/10.1108/0961553121 1231262

Athani SS, Solanki CH, Dodagoudar GR (2015) Seepage and stability analyses of earth dam using finite element method. Aquat Procedia 4:876–883. https://doi.org/10.1016/j.aqpro.2015.02.110

Bahrampour M, Hamzehei-Javaran S, Shojaee S (2018) New insight into viscoelastic finite element modeling of time-dependent material creep problems using spherical Hankel element framework. Int J Appl Mech 10(8):1850085. https://doi.org/10.1142/S1758825118500850

Bereslavskii EN (2011) Simulation of seepage flows from channel. J Appl Math Mech 75(4):398–403. https://doi.org/10.1016/j.jappmathmech.2011.09.004

Buhmann MD (2003) Radial basis functions: theory and implementation. Cambridge University.

Farmani S, Ghaeini-Hessaroeyeh M, Hamzehei Javaran S (2018) The improvement of numerical modeling in the solution of incompressible viscous flow problems using Finite Element Method based on spherical Hankel shape functions. Int J Numer Meth Fluid 87(2):70–89. https://doi.org/10.1002/fld.4482

Farmani S, Ghaeini-Hessaroeyeh M, Hamzehei-Javaran S (2019a) Increasing the solution accuracy in the numerical modeling of boundary value problems using finite element method based on Hankel shape functions. Int J Appl Mech 11(7):1950062. https://doi.org/10.1142/S1758825119500625

Farmani S, Ghaeini-Hessaroeyeh M, Hamzehei-Javaran S (2019b) Developing new numerical modeling for sloshing behavior in two-dimensional tanks based on nonlinear finite element method. J Eng Mech 145(12):04019107. https://doi.org/10.1061/(ASCE)EM.1943-7889.0001686

Farmani S, Ghaeini-Hessaroeyeh M, Hamzehei-Javaran S (2021) Investigating performance of tuned liquid damper using finite-element method based on Lagrange and Hankel functions with nonlinear boundary conditions. J Eng Mech 147(11):04021083. https://doi.org/10.1061/(ASCE)EM.1943-7889.0001993

Fu J, Sheng J (2009) A study on unsteady seepage flow through dam. J Hydrodynam 21(4):499–504. https://doi.org/10.1016/S1001-6058(08)60176-6

Fukuchi T (2016) Numerical analyses of steady-state seepage problems using the interpolation finite difference method. Soil Found 56(4):608–626. https://doi.org/10.1016/j.sandf.2016.07.003

Hamzeh Javaran S, Khaji N, Noorzad A (2011a) First kind Bessel function (J-Bessel) as radial basis function for plane dynamic analysis using dual reciprocity boundary element method. Acta Mech 218:247–258. https://doi.org/10.1007/s00707-010-0421-7

Hamzeh Javaran S, Khaji N, Moharrami H (2011b) A dual reciprocity BEM approach using new Fourier radial basis functions applied to 2D elastodynamic transient analysis. Eng Anal Bound Elem 35(1):85–95. https://doi.org/10.1016/j.enganabound.2010.05.014

Hamzehei Javaran S, Khaji N (2012) Inverse multiquadric (IMQ) function as radial basis function for plane dynamic analysis using dual reciprocity boundary element method. In: 15th world conference on earthquake engineering, Lisboa, Portugal

Hamzehei Javaran S, Khaji N (2014) Dynamic analysis of plane elasticity with new complex Fourier radial basis functions in the dual reciprocity boundary element method. Appl Math Model 38(14):3641–3651. https://doi.org/10.1016/j.apm.2013.12.010

Hamzehei Javaran S, Shojaee S (2017) The solution of elasto static and dynamic problems using the boundary element method based on spherical Hankel element framework. Int J Numer Methods Eng 112(13):2067–2086. https://doi.org/10.1002/nme.5595

Jiang QH, Deng SS, Zhou CB, Lu WB (2010) Modeling unconfined seepage flow using three-dimensional numerical manifold method. J Hydrodynam 22(4):554–561. https://doi.org/10.1016/S1001-6058(09)60088-3

Jiang T, Zhang J, Wan W, Cui S, Deng D (2017) 3D transient numerical flow simulation of groundwater bypass seepage at the dam site of Dongzhuang hydro-junction. Eng Geol 231:176–189. https://doi.org/10.1016/j.enggeo.2017.10.022

Juanes R (2005) A variational multiscale finite element method for multiphase flow in porous media. Finite Elem Anal Des 41(7–8):763–777. https://doi.org/10.1016/j.finel.2004.10.008

Karay G, Hajnal G (2015) Modelling of ground water flow in fractured rocks. Aquat Procedia 25:142–149. https://doi.org/10.1016/j.proenv.2015.04.020

Kazemzadeh-Parsi MJ, Daneshmand F (2013) Three dimensional smoothed fixed grid finite element method for the solution of unconfined seepage problems. Finite Elem Anal Des 64:24–35. https://doi.org/10.1016/j.finel.2012.09.001

Khaji N, Hamzehei Javaran S (2013) New complex Fourier shape functions for the analysis of two-dimensional potential problems using boundary element method. Eng Anal Bound Elem 37(2):260–272. https://doi.org/10.1016/j.enganabound.2012.11.001

Lande CK, Warke BRK, A (2016) Simulation of 2-dimensional subsurface seepage flow in an anisotropic porous medium. Recent Trends Eng Mater Sci 8:276–278. https://doi.org/10.1016/j.pisc.2016.04.051

Lam L, Fredlund DG, Barbour SL (1987) Transient seepage model for saturated-unsaturated soil system: a geotechnical engineering approach. Can Geotech J 24:565–580. https://doi.org/10.1139/t87-071

Mousavi M, Hamzehei-Javaran S, Shojaee S (2021) A new insight into analysis of linear elastic fracture mechanics with spherical Hankel boundary elements. Theor Appl Fract Mech 115:103059. https://doi.org/10.1016/j.tafmec.2021.103059

Pedroso DM (2015) A solution to transient seepage in unsaturated porous media. Comput Methods Appl Mech Eng 285:791–816. https://doi.org/10.1016/j.cma.2014.12.009

Reddy JN (2004) An introduction to the finite element methods, 3rd edn. Oxford University Press, New York

Yang QC, Liang J, Yang ZP (2012) Numerical modeling of groundwater flow in Daxing (Beijing), China. Energy Procedia 14:1671–1676

Yuan S, Zhong H (2016) Three dimensional analysis of unconfined seepage in earth dams by the weak form quadrature element method. J Hydrol 533:403–411. https://doi.org/10.1016/j.jhydrol.2015.12.034